Room-temperature giant magnetoresistance over one billion percent in a bare graphene nanoribbon device

Rui Qin,[1] Jing Lu,[1,*] Lin Lai,[1] Jing Zhou,[1] Hong Li,[1] Qihang Liu,[1] Guangfu Luo,[1,2] Lina Zhao,[3] Zhengxiang Gao,[1] Wai Ning Mei,[2] and Guangping Li[4]

[1]*State Key Laboratory of Mesoscopic Physics and Department of Physics, Peking University, Beijing 100871, People's Republic of China*

[2]*Department of Physics, University of Nebraska at Omaha, Omaha, Nebraska 68182-0266, USA*

[3]*Institute of High Energy Physics, Chinese Academy of Science, Beijing 100049, China*

[4]*SICAS Center, Lee Hall, SUNY Oneonta, Oneonta, New York 13820, USA*

(Received 30 March 2010; published 14 June 2010)

We provide *ab initio* study on a spin valve device that is based on bare ferromagnetic zigzag-edged graphene nanoribbons. Giant magnetoresistance over one billion percent at room temperature is obtained, which is an ultrahigh magnetoresistance among graphene-related spin valve devices and seven orders of magnitude larger than the available experimental values. The orbital parity mismatching between the σ and π^* bands and enhanced exchange splitting due to the dangling bond are two indispensable factors to generate this large magnetoresistance.

DOI: 10.1103/PhysRevB.81.233403 PACS number(s): 73.63.−b, 71.15.Mb, 71.20.Tx, 73.22.−f

Graphene has a long spin relaxation time and length[1–6] due to a small spin-orbit coupling of carbon atoms, and this makes graphene a promising material in applications of spintronics. The most popular existing spintronic devices are spin valves. Graphene-based spin valves have been experimentally constructed, but the resulting magnetoresistance is quite small. A 10% magnetoresistance (MR) is observed in a spin valve with a graphene wire contacted by two soft magnetic electrodes at 300 K.[7] A spin valve consisting of a graphene flake and ferromagnetic electrodes shows a 12% MR at 7 K when a MgO tunnel barrier is inserted at the graphene/electrode interface.[8] Raising magnetoresistance is highly desired for application of graphene in spintronics.

One possible scheme to generate high magnetoresistance is to use zigzag-edges graphene nanoribbons (ZGNRs), which have magnetic moment on the two edges. Spin in each edge of ZGNRs is ferromagnetically coupled.[9,10] The ground states of ZGNRs have the two edges antiferromagnetically coupled, and a gap is opened in the band structure. Ferromagnetic coupling between the two edges of ZGNRs produces a metallic state, which is slightly higher in energy than the ground state. The parallel spin polarization of the two edges can be stabilized by applying an experimentally accessible magnetic field.[11,12] Spin valve can be constructed by either using a ferromagnetic ZGNR connected to two ferromagnetic electrodes [Fig. 1(a)][11] or using an antiferromagnetic ZGNR connected to two metal electrodes.[12] The former device functions via changing the relative direction of the local magnetic field applied on the electrodes and the latter does by applying a magnetic field on the antiferromagnetic ZGNR. Giant MR is predicted in the two spin valves. Especially, an impressive giant MR of over one million percent at room temperature and thousands of times larger than the experimental values is predicted in the first type spin valve when using H-terminated ZGNRs,[11] as a result of orbital symmetry mismatch of the energy bands with respect to the ribbon midplane on the two leads.

It is well known that edge modulation affects the electronic structure of ZGNRs. Two questions arise: whether higher MR is available in ZGNR-based spin valve by edge modulation and what is the possible limit room-temperature MR of graphene-based spin valves. Dehydrogenation and passivation by other groups are two schemes of edge modulation. Bare graphene nanoribbons can exist in the laboratory and they are stable even at sufficiently high temperature of 2000 K from the tight-binding molecular-dynamics simulation.[13] In this Brief Report, we use a bare ZGNR to connect to two ferromagnetic electrodes and dramatically raise room-temperature MR to over one billion percent from *ab initio* transport calculations. This renders bare ZGNRs more attractive than H-passivated ones for nanospintronics.

We use *N*-ZGNR to denote a ZGNR with *N* zigzag chains, and different bare *N*-ZGNRs ($N=2$, 4, 6, 8, 12, 16, and 24) with width $w_{\text{ribbon}}=0.3-5.0$ nm are considered. Experimentally, GNRs with widths down to sub-10 nm have been synthesized.[14,15] The geometry optimization and electronic structures are calculated by using the density-functional theory (DFT) implemented in the ATK code.[16–18] The quantum transport properties are computed by using the DFT coupled with the nonequilibrium Green's function (NEGF) formalism also implemented in the ATK code. The local density approximation (LDA) and norm-conserving pseudopotentials of the Troullier-Martins type[19] are used. Single-ζ polarization basis sets are used for the ZGNRs with small width ($N\leq 6$), while single-ζ basis sets are used for the ZGNRs with large width ($N>6$). The mesh cutoff is chosen as 400 Ry. Since the practical spin valves usually work at room temperature, the electron temperature is set to 300 K in our calculations. The structures of the ZGNRs are optimized until the maximum atomic forces are less than 0.03 eV/Å. Sufficiently large scattering region is needed to get the converged transmission spectra. For example, scattering region of 24 unit cells is required for the bare 4-ZGNR based spin valve. The orbital wave functions are calculated with double numeric with polarization basis sets implemented in the DMol^3 package.[20,21] In our calculations, the contact resistance and spin flip processes are supposed to be negligible.

The spin-resolved current I_σ under bias voltage V_{bias} is

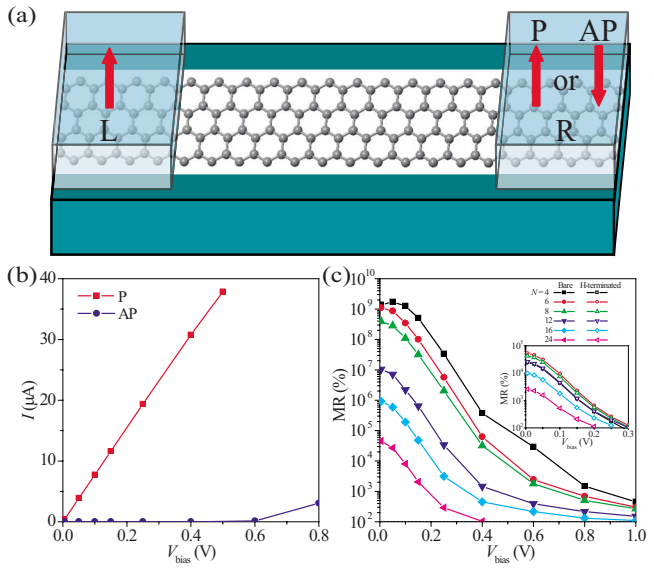

FIG. 1. (Color online) (a) Schematic model of a bare ZGNR-based spin valve device. The spin polarization directions (arrows) of the two ferromagnetic electrodes [light blue (light gray) areas] can be controlled by the magnetic field. P and AP denote the configurations, in which the spin polarization directions of the two electrodes are parallel and antiparallel, respectively. (b) *I-V* characteristics of the bare 4-ZGNR in the P and AP configurations. (c) Bias dependence of the magnetoresistances of the bare *N*-ZGNRs. Inset: bias dependence of the magnetoresistances of the H-terminated *N*-ZGNRs. The magnetoresistances of both the bare and H-terminated 2-ZGNRs nearly vanish and are not shown in the figure.

calculated with the Landauer-Büttiker formula,[22]

$$I_\sigma(V_{\text{bias}}) = \frac{e}{h}\int_{-\infty}^{\infty}[T_\sigma(E,V_{\text{bias}})\{f_{\text{L}}(E,V_{\text{bias}}) - f_{\text{R}}(E,V_{\text{bias}})\}]dE, \tag{1}$$

where $T_\sigma(E,V_{\text{bias}})$ is the spin-resolved transmission probability, $f_{\text{L/R}}(E,V_{\text{bias}})$ is the Fermi-Dirac distribution function for the left (L)/right (R) electrode, and σ is a spin index.

The current in the parallel (P) configuration I_{P} is found significantly greater than its counterpart in the antiparallel (AP) configuration I_{AP}. The current in the P configuration linearly increases under low bias voltage, and the conductance is found quantized ($2e^2/h$), regardless of the ribbon width. In contrast, the current in the AP configuration is very small till certain threshold voltage. The *I-V* curves of the bare 4-ZGNR case are shown in Fig. 1(b). Magnetoresistance is calculated from the *I-V* characteristics by using the definition $\text{MR}=(I_{\text{P}}-I_{\text{AP}})/I_{\text{AP}}$, and the resulting voltage dependent MR curves of bare ZGNRs with different width *N* at 300 K are shown in Fig. 1(c). The MRs of bare ZGNR-based devices generally decrease with the increasing bias and width *N*. One exception is the MR of the bare 4-ZGNR case, which first increases slightly before it starts to decay at 0.05 V. Strikingly, the MRs at a small bias of 0.005 V have ultrahigh values of $4.5\times10^4\%-1.4\times10^9\%$. The maximum experimental MR values at room temperature are a few hundred percent,[23–25] and our theoretical MRs of the bare ZGNR-based devices are thus two to seven orders of magnitude much larger than the available experimental values. For comparison, we also investigated the MRs of the H-terminated ZGNR based devices and show the results in inset of Fig. 1(c). The MRs of the H-terminated ZGNR-based devices decrease monotonically with the increasing bias, but the MR peaks at $N=6$ and then decreases with the increasing *N*. The MRs of the H-terminated ZGNRs are $2.6\times10^3\%-5.3\times10^4\%$ at 0.005 V, which are one to five orders of magnitude smaller than those of their respective bare counterparts. Our MRs of the H-terminated ZGNRs are compared with MRs of about $1.2\times10^4\%-1.2\times10^6\%$ at 0.005 V bias for the H-terminated ZGNRs with width $N=8$, 16, 24, and 32 obtained by Kim *et al.*[11]

In the P configuration, the transmission spectra of the bare and H-terminated ZGNRs at zero bias show conventional perfect transmission [left panels in Figs. 2(a) and 2(b)]. As the bias increases, the transmission probability remains to be one around the Fermi level (E_f) for both spins. Thus, the *I-V* curve in the P configuration is linear. In the AP configuration, the transmission spectra of two spins are degenerate at zero bias, and a zero transmission gap (ZTG) appears around E_f [left panels in Figs. 2(c) and 2(d)]. As the bias increases, ZTG of α spin decreases, while that of β spin increases [Fig. 3(a)] (α and β are the majority and minority spins, respectively). I_{AP} thus has ultra small values and increases nearly exponentially under low bias, which results in the high MR and the decay of MR with the increasing bias.

The MRs at 0.005 V for different both bare and H-terminated *N*-ZGNRs devices are plotted in Fig. 3(b) as a function of the ZTG. The MRs are found to increase nearly

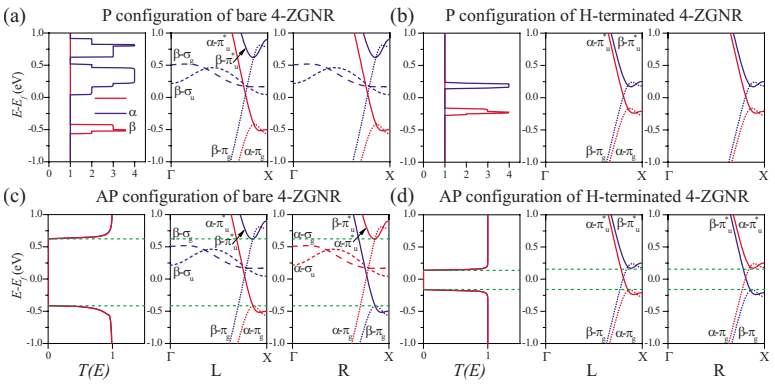

FIG. 2. (Color online) Spin-resolved transmission spectra and band structures of the left (l) and right (r) leads (a)/(b) in the P configuration of the ferromagnetic bare/H-terminated 4-ZGNR-based spin valve device at zero bias. (c) and (d) The same as (a) and (b), but for the AP configuration. The areas between the dash lines in the transmission spectra and the band structures denote the ZTG and the SOSMA, respectively.

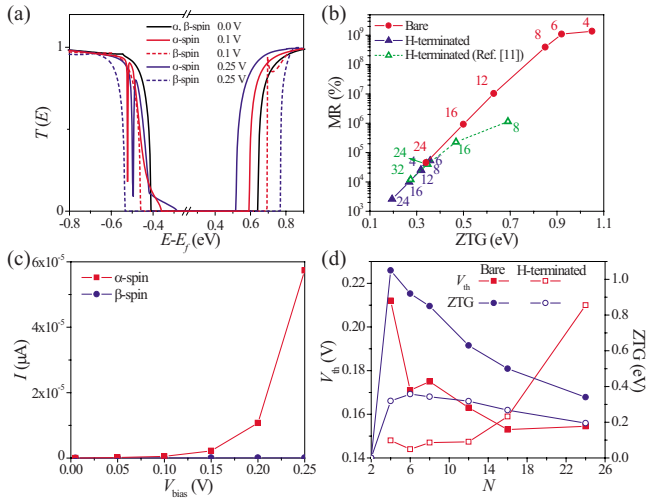

FIG. 3. (Color online) (a) Spin-resolved transmission spectra of the bare 4-ZGNR in the AP configuration at biases of 0, 0.1, and 0.25 V. The transmission spectra are degenerate for the two spins at zero bias. (b) Magnetoresistance at $V_{\text{bias}}=0.005$ V as a function of the ZTG for different N-ZGNR. The number denotes the ribbon width N. The results of the H-terminated 4- and 12-ZGNR are almost superposed. (c) Spin-resolved I-V curve for the bare 4-ZGNR in the AP configuration. (d) V_{th} (see text) and ZTG of the bare and H-terminated ZGNRs as a function of the ribbon width N.

exponentially with the increasing ZTG when ZTG is smaller than about 0.9 eV. Since only the overlapping area between the exponential tail of $f_L - f_R$ and the transmission curve contributes to the current at the AP configuration, I_{AP} decreases nearly exponentially with the increasing ZTG, and thus MR increases nearly exponentially with the increasing ZTG. The larger MRs for the bare ZGNRs than for the H-terminated ZGNRs are thus attributed to the larger ZTGs in the bare ZGNRs. The bare 4-ZGNR has the largest ZTG of 1.05 eV and thus has the largest MR. The H-terminated 6-ZGNR has the largest ZTG of 0.36 eV in the H-terminated ZGNRs and thus has the largest MR in the H-terminated ZGNRs. The ZTGs of the H-terminated ZGNRs obtained by Kim *et al.*[11] are also shown in Fig. 3(b) and they are somewhat larger than ours, which accounts for their larger MRs than ours.

The band structures of the two leads in P/AP configurations for the ferromagnetic bare 4-ZGNR at zero bias are shown in the central and right panels of Fig. 2(a) and 2(c), respectively. For comparison, the corresponding band structures of the H-passivated 4-ZGNR are shown in the central and right panels of Figs. 2(b) and 2(d), respectively. Around E_f are the π^* (higher-lying) and π (lower-lying) bands. Besides the π^* and π bands, two additional narrow bands appear near E_f for the bare 4-ZGNR and are identified as σ bands from their wave functions, whose signs are unchanged when rotating about the bonding direction [Figs. 4(c) and 4(d)]. We further distinguish the π^*, π, and σ bands with a subscript g and u, which represent even and odd parity with respect to the inversion through the origin, respectively. When the ribbon width N is even, the orbitals of the energy bands have definite parity under the yz midplane mirror operation [Fig. 4(a)].[11,26] The orbitals of the π_u^* and σ_g bands have even parity under the yz mirror operation [Figs. 4(a) and 4(c)], while those of the π_g and σ_u bands have odd parity [Figs. 4(b) and 4(d)]. On the other hand, the σ orbitals originate from the hybridization of the s, p_x, and p_y orbitals and have even parity under the xz mirror operation [Figs. 4(c) and 4(d)]; the π/π^* orbitals originate from the hybridization of the p_z orbitals and have odd parity under the xz mirror operation [Figs. 4(a) and 4(b)].

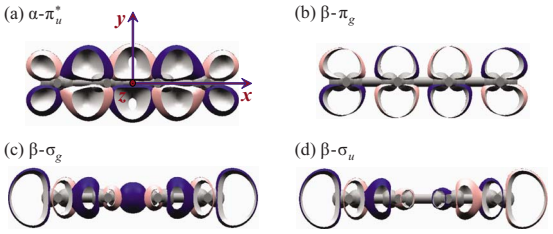

FIG. 4. (Color online) (a)–(d) Isosurfaces of the wave functions of the states at the Γ points of the α-π_u^*, β-π_g, β-σ_g, and β-σ_u bands for the bare 4-ZGNR, respectively. The coordinate system is shown in (a). The isovalue is 0.03 a.u. Pink (light gray) and dark blue (deep gray) indicate opposite signs of the wave functions.

In a traditional spin valve, the transmission is only driven by spin matching. In the ZGNR device, the transmission also depends on the orbital symmetry matching of the energy bands. The transmission is allowed only when both the spin and orbital symmetry of the energy bands on the two leads are matched, otherwise is forbidden. Therefore, the ZTG is equal to the energy area where either of the spin and orbital symmetry of all the bands between the two leads in this area is mismatched [we refer to it as spin orbital-symmetry mismatching area (SOSMA)]. The SOSMA in the H-terminated ZGNRs is determined by the spin mismatching and parity mismatching of the orbitals with respect to the yz mirror.[11] By contrast, in the bare ZGNR case, although the π_u^* and σ_g bands of β spin have the same even parity about the yz mirror, the transmission between them remains forbidden because the orbitals of the π_u^* and σ_g bands have odd and even parity, respectively, under the xz mirror operation. Therefore, the SOSMA in the bare ZGNRs is determined by the spin mismatching and parity mismatching of the orbitals with respect to both the yz mirror and the xz mirror. The additional symmetry mismatching about the xz mirror is one factor responsible for the significantly larger SOSMA and ZTG in the bare ZGNRs than those in their H-passivated counterparts. The other factor is associated with the larger exchange splitting in the bare ZGNRs.

From Fig. 2, the value of the SOSMA is actually equal to the energy difference, Δ, between the bottom of the π^* band of the β spin and the top of the π band of the α spin. Δ is furthermore nearly equal to the exchange splitting, Δ_{ES}, of the π^* band at the band minimum (or the π band at the band maximum). Taken together, we have

$$\text{ZTG} = \text{SOSMA} = \Delta \cong \Delta_{ES}. \tag{2}$$

The dangling bond in the bare ZGNRs greatly enhances the total magnetic moment of ZGNRs and thus greatly enhances exchange splitting Δ_{ES},[27,28] ZTG, and MR. Taking the 4-ZGNR as an example, the total magnetic moments of the

bare and H-terminated 4-ZGNRs are $2.4\mu_B$ and $0.4\mu_B$ per unit cell, respectively, and the corresponding Δ_{ES} values are about 1.1 and 0.4 eV, respectively. The state at the bottom of the π^* band is an extended state, and Δ_{ES} scales with the weight of the edge sites in this bottom extended state of the π^* band. When N increases, the weight of the edge sites decreases, yielding a decrease in Δ_{ES} (Ref. 29) and ZTG when $N>2$ in the bare ZGNRs and $N>4$ in the H-terminated ZGNRs. As for the narrowest 2-ZGNR, there is a large overlap of the π^* and π bands of the same spin channel because of a strong interaction between the two quite close edges. Consequently the top of the π band of the α spin surpasses the bottom of the π^* band of the β spin and leads to a closing of Δ and ZTG.[30]

We also find SOSMA of the ketone-, hydroxyl-, nitryl-, amine-, lactone-, and ether-passivated 6-ZGNRs are 0, 0.08, 0.18, 0.17, 0.09, and 0 eV, respectively, which are smaller than SOSMA of the H-passivated 6-ZGNR of 0.36 eV. Thus no greater MR is expected. Preliminary calculations show that the room-temperature MRs of the second type ZGNR spin valve at finite bias are only a few thousand percent, much smaller that those of the first type ZGNR spin valve. Thus the MR over one billion percent obtained in the first type bare ZGNR-based spin valve is an extremely large room-temperature MR of graphene-related spin valves, in light of the fact that bare ZGNRs have large total magnetic moments of ZGNRs.

The opposite behaviors of ZTGs of the two spins with the increasing bias in the AP configuration cause spin-polarized current at the finite bias.[11] The spin-polarized I-V curves in the AP configuration of the bare 4-ZGNR are shown in Fig. 3(c). As the bias increases, the α spin current increases nearly exponentially, while the β spin current remains nearly zero. Taking the definition of spin filter efficiency (SFE) $=(I_\alpha - I_\beta)/(I_\alpha + I_\beta)$, the SFE of the ZGNRs increases to nearly 100% with the increasing bias. We define a threshold voltages V_{th} to generate 99% SFE. As shown in Fig. 3(d), in general, V_{th} of the bare ZGNRs decreases with the increasing N, while that of the H-terminated ZGNRs increases with the increasing N.

In conclusion, dehydrogenation is found to greatly increase the zero transmission gap and drastically raise magnetoresistance of a ZGNR-based spin valve by several orders of magnitude from *ab initio* transport calculations. These theoretical MRs can be viewed as the upper limits of realistic observations because defects, contact resistance and spin flip processes, etc., are not considered in our model. The increase in the zero transmission gap upon dehydrogenation is attributed to the additional symmetry mismatching between the σ and π^* bands about the ribbon plane on the two leads and the significantly enhanced exchange splitting by the dangling bond.

This work was supported by the NSFC (Grants No. 10774003, No. 10474123, No. 10434010, No. 90626223, and No. 20731162012), National 973 Projects (Grant No. 2007CB936200, MOST of China), Fundamental Research Funds for the Central Universities, Program for New Century Excellent Talents in University of MOE of China, National Foundation for Fostering Talents of Basic Science (Grant No. J0630311), and Nebraska Research Initiative (Grant No. 4132050400) of USA. We thank K. Xia for helpful discussion.

*jinglu@pku.edu.cn

[1] C. Berger *et al.*, J. Phys. Chem. B **108**, 19912 (2004).
[2] K. S. Novoselov *et al.*, Science **306**, 666 (2004).
[3] K. S. Novoselov *et al.*, Nature (London) **438**, 197 (2005).
[4] C. Berger *et al.*, Science **312**, 1191 (2006).
[5] A. K. Geim and K. S. Novoselov, Nat. Mater. **6**, 183 (2007).
[6] K. S. Novoselov *et al.*, Phys. Status Solidi B **244**, 4106 (2007).
[7] E. W. Hill *et al.*, IEEE Trans. Magn. **42**, 2694 (2006).
[8] W. H. Wang *et al.*, Phys. Rev. B **77**, 020402(R) (2008).
[9] Y.-W. Son *et al.*, Phys. Rev. Lett. **97**, 216803 (2006).
[10] Y.-W. Son *et al.*, Nature (London) **444**, 347 (2006).
[11] W. Y. Kim and K. S. Kim, Nat. Nanotechnol. **3**, 408 (2008).
[12] F. Muñoz-Rojas *et al.*, Phys. Rev. Lett. **102**, 136810 (2009).
[13] T. Kawai *et al.*, Phys. Rev. B **62**, R16349 (2000).
[14] X. Wang *et al.*, Phys. Rev. Lett. **100**, 206803 (2008).
[15] L. Jiao *et al.*, Nature (London) **458**, 877 (2009).
[16] ATOMISTIX Toolkit version 2008.10, QuantumWise A/S (www.quantumwise.com).
[17] J. Taylor *et al.*, Phys. Rev. B **63**, 245407 (2001).
[18] M. Brandbyge *et al.*, Phys. Rev. B **65**, 165401 (2002).
[19] N. Troullier and J. L. Martins, Phys. Rev. B **43**, 1993 (1991).
[20] B. Delley, J. Chem. Phys. **92**, 508 (1990).
[21] B. Delley, J. Chem. Phys. **113**, 7756 (2000).
[22] S. Datta, *Electronic Transport in Mesoscopic Systems* (Cambridge University Press, Cambridge, England, 1995).
[23] S. S. P. Parkin *et al.*, Nat. Mater. **3**, 862 (2004).
[24] S. Yuasa *et al.*, Nat. Mater. **3**, 868 (2004).
[25] S. Ikeda *et al.*, Appl. Phys. Lett. **93**, 082508 (2008).
[26] Z. Li *et al.*, Phys. Rev. Lett. **100**, 206802 (2008).
[27] H. Lee *et al.*, Phys. Rev. B **72**, 174431 (2005).
[28] H. Lee *et al.*, Chem. Phys. Lett. **398**, 207 (2004).
[29] J. Jung *et al.*, Phys. Rev. Lett. **102**, 227205 (2009).
[30] See supplementary material at http://link.aps.org/supplemental/10.1103/PhysRevB.81.233403 for the band structures of the ferromagnetic bare and H-terminated two-ZGNRs.